TRANSPORTES
www.revistatransportes.org.br
anpet
associação nacional de pesquisa e ensino em transportes
www.anpet.org.br

# Numerical simulation of geogrid reinforced flexible pavements

## *Avaliação numérica da influência da geogrelha no desempenho de pavimentos flexíveis*

**Gabriel Orquizas Mattielo Pedroso**[1], **Jefferson Lins da Silva**[2]

[1]University of São Paulo, São Paulo - Brazil, gabpedroso@usp.br
[2]University of São Paulo, São Paulo - Brazil, jefferson@sc.usp.br

**Recebido:**
25 de abril de 2020
**Aceito para publicação:**
3 de julho de 2020
**Publicado:**
22 de julho de 2021
**Editor de área:**
Francisco Thiago Aragão

**Keywords:**
Geogrid.
Reinforcement.
Flexible pavement.
Permanent deformation.

**Palavras-chave:**
Geogrelha.
Reforço.
Pavimento Flexível.
Deformação Permanente.

DOI:10.14295/transportes.v29i1.2366



**ABSTRACT**
This paper aims to develop a mechanistic analysis methodology in finite elements, using the ABAQUS program, to investigate the influence of geogrids as a reinforcement element in the performance of flexible pavements. To do this, an analytical methodology was adopted to calculate the additional confining stress provided by the reinforcement. The behavior of the base and subgrade materials was considered non-linear through a writing Fortran routine. An interface element between the geogrid and geotechnical material was also considered. The value of permanent deformation modeled numerically was compared with experimental results, which shows that the adopted methodology had a satisfactory fit. Thereby, different pavement configurations were simulated and analyzed. The parametric results show that by inserting a geogrid as an element to improve the pavement mechanical response, mainly due to the reduction of vertical stresses in the reinforcement layer and, consequently, the permanent deformation helps to prolong the paving service life.

**RESUMO**
O objetivo deste trabalho é desenvolver uma metodologia de análise mecanicista em elementos finitos, no programa ABAQUS, para investigar a influência da geogrelha como elemento de reforço no desempenho de pavimentos flexíveis. Para isso, uma metodologia analítica foi adaptada para o cálculo do acréscimo de confinamento lateral proporcionado pelo reforço, também foi considerado o comportamento não linear dos materiais de base e subleito, por meio da introdução de uma sub-rotina escrita em linguagem Fortran, e adotou-se as devidas propriedades de interface entre geogrelha e material geotécnico. Os resultados de afundamento na trilha de roda modelados e experimentais foram comparados, mostrando que a metodologia adotada apresentou um ajuste satisfatório. Com isso, diferentes configurações de pavimento foram simuladas e avaliadas. Os resultados evidenciam que a inserção da geogrelha como elemento de reforço melhora a resposta do pavimento, principalmente por diminuir as tensões verticais na camada em que está inserida e consequentemente a deformação permanente, o que resulta no aumento da vida útil do pavimento.

## 1. INTRODUCTION

Most Brazilian pavements are classified as flexible, and the main function of these flexible pavements is to allow traffic load redistribution from the surface to the underlying layers. Therefore, when following a design, two types of rupture are taken into account: a) Fatigue - located in the layer with the largest resilient module and caused by alternate flexion of the layer during the traffic load, b) Permanent deformation - resilient vertical displacement of each pavement layer, which can cause rutting damage on the pavement surface. Thus, the layers must have sufficient

thickness and stiffness to limit their excessive vertical deformation (Yoder and Witczak, 1975).

One of the most widespread ways of dimensioning pavements and which is constantly being studied are mechanistic empirical pavement design methods. These methods are based on stresses, strains and displacements of the pavement structure subjected to traffic. Among different mechanistic methods of pavement response that can be used, the multilayer elastic theory (MLET) and the finite element method (FEM) are the most common. The ABAQUS finite element program has been used in the academic environment to study pavement stresses and strains, as it allows the modeling of nonlinear material behavior, forms of loading and interface elements (Santos *et al*., 2019).

A subgrade is natural soil at a construction site, and according to Vertematti (2015) in some flexible pavement structures, an unbound granular layer is placed directly above a low support subgrade. This can lead to damage on the pavement, such as: rutting due to excess deformation of the pavement layers; or fatigue cracking, which may be associated with the migration of fines from the subgrade and the penetration of the granular base layer into the subgrade.

In the presence of weak subgrade, laboratory studies have shown the benefit of using a geogrid as reinforcement (Kakuda *et al*., 2011 and Costa *et al*., 2017). These studies indicate a decrease in vertical displacements in the pavement structure and, consequently, a reduction in permanent deformation.

In this context, according to Perkins and Ismeik (1997), the performance of geosynthetic reinforcement in flexible pavements is due to the lateral confinement mechanism, in which the interaction between the base granular material and the geosynthetic reinforcement allows the transfer of stress from the base to the geosynthetic. Therefore, the function of the geosynthetic is to avoid the horizontal displacement of the material, maintaining its confinement.

According to Kwon *et al*. (2005), the design using geosynthetic reinforcement needs to be incorporated into mechanistic empirical analysis, as it is the most suitable alternative to evaluate the effectiveness and benefits of the presence of geosynthetics in the pavement structure. However, there is a difficulty in quantifying the additional confining stress applied from the geosynthetic in the unbound granular material. To account for the increase in confining stress, in FEM analyses, studies such as those by Nazzal *et al*. (2010); Abu-Farsakh *et al*. (2014) and Tang *et al*. (2016) proposed an increase in the geosynthetic modulus, when compared with that obtained in the laboratory. Moreover, Kwon *et al*. (2005) empirically added a horizontal stress in the reinforced area. In addition, Perkins *et al*. (2009) presented a numerical model in two stages. The first is a compaction model, which resulted in increases in horizontal stresses in the reinforced layer and the second stage considers the horizontal stresses from the compaction model and the traffic load. On the other hand, Yang and Han (2013) and Gu *et al.* (2016) proposed an analytical model to calculate the additional confining stress provided by the reinforcement based on the results of repeated triaxial compression tests.

In Brazil, with the evolution of mechanistic design methods for flexible pavements and the introduction of the SisPav program proposed by Franco (2007), there is a need to incorporate geogrid reinforcement in these analyses. In this context, this article aims to adapt the methodology proposed by Yang and Han (2013) and Gu *et al*. (2016) regarding the mechanistic design of flexible pavements incorporating geosynthetic reinforcement, of the geogrid type, using the ABAQUS program. Furthermore, this paper aims to compare the results obtained by the proposed model with the results of the experimental model by Kakuda (2010). Finally, based on the proposed numerical model, the influence of the geogrid stiffness, the

location of the reinforcement and the interface parameters on the performance of the simulated pavements is evaluated.

## 2. NUMERICAL ANALYSIS IN FINITE ELEMENTS OF FLEXIBLE PAVEMENT REINFORCED WITH GEOGRID

Finite element analyses were performed using the ABAQUS program to predict the pavement response (stresses and strains), and thus, estimate its long-term performance (total permanent deformation) with the permanent deformation model proposed by Guimarães (2009).

Similar to the studies carried out by Nazzal *et al*. (2010), Abu-Farsakh *et al*. (2014) and Tang *et al*. (2016), an axisymmetric analysis was adopted whereby the pavement layers were modeled as a solid 8-node element and the geogrid as a 3-node membrane element, both with reduced integration. To minimize the edge effects, a width of 2.4 m was considered as the model and 1.4 m as the depth of the subgrade, which represent approximately 15 and 10 times the diameter of the wheel loading area, respectively.

To optimize the simulation, the mesh density next to the wheel loading was increased and near the edges of the model it was decreased. The boundary conditions were adopted to prevent vertical and horizontal displacement at the bottom of the model and horizontal displacement at the sides.

As exemplified in Santos *et al.* (2019), the interface between layers in ABAQUS (2014) is defined through the contact among two nodes and two adjacent surfaces belonging to the finite element mesh. Furthermore, it is represented by the Coulomb Equation (Equation 1).

$$\tau_{crit} = \mu . p \quad (1)$$

where $\tau_{crit}$: interface shear stress;

$\mu$: interface friction coefficient; and

$p$: contact pressure between the surfaces.

In Equation 1, the friction coefficient μ can vary between 0 and 1, whereby the value of 0 allows the free displacement between the layers, thus 1 corresponds to the layers that are bonded. In this study, the non-bounded condition was adopted for the interface between layers, and for the reinforcement interfaces, the experimental values available in Marques (2018) were adopted.

As the objective of this paper is to evaluate the permanent deformation of the layers below the asphaltic surface on a flexible pavement, a verification on fatigue has not been incorporated. Therefore, in the model verification stage, based on the adopted experimental reference results, there is no asphalt surface. However, afterwards, in the parametric analysis there is a presence of an asphalt surface, which was modeled using an elastic linear model.

### 2.1. Resilient and permanent deformation models of base and subgrade materials

Under the repeated application of traffic loads, most of the pavement deformations are recoverable and considered elastic. Therefore, the Resilient Modulus ($M_R$) is defined for the materials elastic stiffness, i.e. the deviation stress $\sigma_d$ divided by the recoverable strain ($\varepsilon_r$), $M_R = \sigma_d / \varepsilon_r$. Repeated load triaxial tests are commonly used to evaluate the resilient modulus.

According to Bernucci *et al*. (2006), it is known that paving materials are not elastic and that they depend on climatic conditions, as well as the stress history. As the stress states vary within a layer, the $M_R$ also changes according to the depth and horizontal distance. To represent the $M_R$

change with the stress state, the Uzan (1988) model shown in Equation 2 considers both the effect of the confining and deviator stress.

$$M_R = K_1 . p_a . \left( \frac{\theta}{p_a} \right)^{k_2} . \left( \frac{\tau_{oct}}{p_a} + 1 \right)^{k_3}$$

$$\theta = \frac{\sigma_{11} + \sigma_{22} + \sigma_{33}}{3} \quad (2)$$

$$\tau_{oct} = \frac{1}{3} \sqrt{\left[ \left( \sigma_{11} - \sigma_{22} \right)^2 + \left( \sigma_{22} - \sigma_{33} \right)^2 + \left( \sigma_{33} - \sigma_{11} \right)^2 \right]}$$

where $M_R$: resilient modulus (MPa);

$\theta$: bulk stress (MPa);

$\tau_{oct}$: octahedral shear stress (MPa);

$p_a$: atmospheric stress (MPa); and

$k_1; k_2; k_3$: repeated triaxial constitutive material parameters.

In ABAQUS, to properly characterize the resilient behavior of pavement materials, the non-linear stress-dependent modulus from the Uzan (1988) model was programmed in a user-defined material (UMAT), which is a subroutine written in Fortran language to characterize the behavior of geotechnical materials. Therefore, the constitutive model in ABAQUS was written in the form of a matrix relating stress and strain.

In this paper, the UMAT equation developed by Hjelmstad and Taciroglu (2000) was used to represent the nonlinear behavior of the materials. According to these authors, the program transmits the stresses, strains, and state variables at the beginning of each time increase together with the current stress increase. The subroutine, therefore, updates the values of stresses and strains and at the end of the time increment provides the material stiffness matrix. The analysis starts with an arbitrary stiffness matrix and the first load increment, then the $M_R$ is calculated, and the convergence condition is verified (the error between the $M_R$ of the previous and current increment must be less than 1%). If convergence is not achieved, a reduction factor of 0.3 is applied to the next increment.

The Guimarães model (2009), synthesized in Equation 3, is used in this paper to calculate permanent deformation, using a nonlinear multiple regression, correlating the confining stress, deviation stress, and loading cycles from a repeat cyclic triaxial test. Moreover, Guimarães *et al*. (2018) showed that the classic permanent deformation models do not present a good correlation for tropical soils, such as Brazilian soils, and that the model proposed in Equation 3 presents better results.

$$\varepsilon_p = \psi_1 . \left( \frac{\sigma_3}{p_a} \right)^{\psi_2} . \left( \frac{\sigma_d}{p_a} \right)^{\psi_3} . (N)^{\psi_4} \quad (3)$$

where $\varepsilon_p$: permanent strain;

$\sigma_3$: confining stress (kPa);

$\sigma_d$: deviator stress (kPa);

$N$: cycles of loading; and

$\psi_1; \psi_2; \psi_3; \psi_4$: repeat load permanent deformation constitutive material parameters.

## 2.2. Analytical model to quantify the additional confining stress

Figure 1 presents a schematic model of a geogrid (gray) reinforced granular base layer subject to traffic load. The granular material is in a stress and strain state, in which it accumulates strains in both axial and radial directions. The radial interaction stress by the granular material and the geogrid generates the tensile stress T, which develops a uniform radial stretch *d* on the geogrid. Then, the geogrid contact friction interlocks the granular material. According to Perkins and Ismeik (1997), the interlocking of granular material in contact with the geogrid is the lateral confinement main reinforcement mechanism.

The interlocking of the granular layer induces in an influence zone with additional confining stress $\Delta\sigma_3$, represented by the letter *h* in Figure 1. Previous studies, such as those by Perkins (2004) and Schuettpelz *et al*. (2009) showed that the influence zone height of the reinforcement varies between 10 and 15 cm.

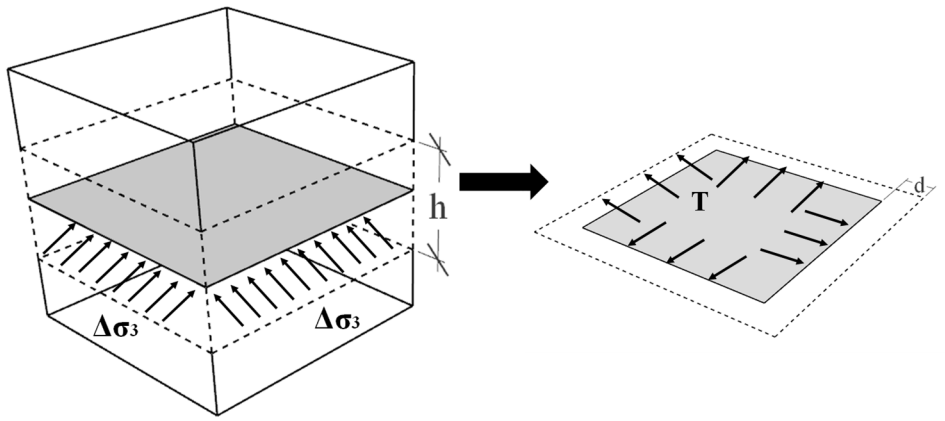


**Figure 1.** Schematic model of geogrid (gray) reinforced granular base layer

Considering the applied forces in the reinforcement as planar and the axisymmetric boundary conditions, the force in reinforcement T can be obtained with Equation 4.

$$T = \frac{E_g}{\left(1-\upsilon_g\right)}.\varepsilon_r^g \tag{4}$$

where *T:* tensile stress development in the geogrid (kN/m);
*$E_g$:* geogrid stiffness (kN/m);
*$\upsilon_g$:* geogrid Poisson's ratio; and
*$\varepsilon_r g$:* geogrid radial strain.

As reported by Tang *et al*. (2013), the geogrid radial strain is a difficult parameter and needs the construction of a fully laboratorial instrumented session to be acquired. Therefore, Yang and Han (2013) proposed the α parameter referring to the bonding between the granular material and geogrid. This parameter correlates the radial strain of the geogrid with the radial strain of the granular material $\alpha = \varepsilon_r^g / \varepsilon_r^a$, where α equal to 1 represents fully bonded and where α equal to 0 the geogrid has no interaction with the granular material. This bonding coefficient value is determined by construction conditions, geogrid opening and granular material diameter.

The additional confining stress Δσ3 is distributed in the influence zone as shown in Figure 1 and can be obtained by dividing force T by the reinforcement influence zone thickness h,

as presented in Equation 5. It should be emphasized that force T developed in the reinforcement is the same throughout its extension and the confinement stress Δσ3 is constant within the influence zone.

$$\Delta\sigma_3 = \frac{T}{h} = \frac{E_g}{\left(1-\upsilon_g\right).h}.\alpha.\varepsilon_r^a \tag{5}$$

where $h$: reinforcement influence thickness (mm);
$\alpha$: bonding coefficient;
$\Delta\sigma_3$: additional confining stress (MPa); and
$\varepsilon_r^a$: granular material radial strain.

In Equation 5, the granular material radial strain $\varepsilon_r^a$ can be divided into an elastic and a plastic portion $\varepsilon_r^a = \varepsilon_{3,p}^a + \varepsilon_{3,e}^a$. According to Yang and Han (2013), the dilatation angle ψ is obtained through cyclic triaxial tests and correlates the radial strain with the axial strain of a specimen. As the dilation angle is a parameter of rare laboratory acquisition and to simplify the use of the model, radial permanent deformation and axial permanent deformation were adopted equivalent to $\varepsilon_{3,p}^a = \varepsilon_{1,p}^a$.

The granular material axial permanent deformation is obtained according to Equation 6, which uses the model proposed by Guimarães (2009).

$$\varepsilon_{3,p}^a = \psi.\varepsilon_{1,p}^a = \psi_1.\left(\frac{\theta}{p_a}\right)^{\psi_2}.\left(\frac{\tau_{oct}}{p_a}+1\right)^{\psi_3}.(N)^{\psi_4} \tag{6}$$

where $\varepsilon_{3,p}^a$: radial permanent deformation;
$\psi$: dilatation angle; and
$\varepsilon_{1,p}^a$: axial permanent deformation.

Equation 7 presents the granular material radial deformation elastic portion, which was obtained through the generalized Hooke's Law. For this, the following simplifications were adopted: 1) the granular material horizontal and vertical elasticity modulus are the same, 2) the Poisson's ratio is the same in all directions.

$$\varepsilon_{3,e}^a = \frac{\left(\sigma_3+\Delta\sigma_3\right)}{E_a} - \frac{\upsilon_a.\sigma_1}{E_a} \tag{7}$$

where $\varepsilon_{3,e}^a$: elastic deformation of the granular material;

Substituting Equations 6 and 7 into Equation 5, we have Equation 8.

$$\Delta\sigma_3 = \frac{E_g.\alpha}{\left(1-\upsilon_g\right).h}.\left[\left[\frac{\left(\sigma_3+\Delta\sigma_3\right)}{M_R} - \frac{\upsilon_a.\sigma_1}{M_R}\right] + \left[\psi_1.\left(\frac{\theta}{p_a}\right)^{\psi_2}.\left(\frac{\tau_{oct}}{p_a}\right)^{\psi_3}.(N)^{\psi_4}\right]\right] \tag{8}$$

Equation 8, referring to the additional confining stress $\Delta\sigma_3$, is an algebraic expression which is the function of the properties form the granular material, the geogrid, and the layer stress state. As the stress state depends on the additional confining stress, a MathCad iterative calculation routine was used to solve it.

The additional confining stress along the reinforcement influence zone causes an increase in the resilience module within this zone. Then, a new resilience modulus value is calculated from Equation 9.

$$M_{R\,reinforced} = k_1 \cdot \left( \frac{\theta}{p_a} + \Delta\sigma_3 \right)^{k_2} \cdot \left( \frac{\tau_{oct}}{p_a} + 1 \right)^{k_3} \quad (9)$$

The theoretical reinforcement influence thickness δ adopted in this paper is 15 cm, however it is also dependent on the location of the reinforcement and the thickness of the layer in which it is inserted. Equation 10 takes these factors into account to determine the effective influence thickness *h'*.

$$h' = \begin{cases} \delta \Leftrightarrow \frac{\delta}{2} < l < H - \frac{\delta}{2} \\ \frac{\delta}{2} + l \Leftrightarrow l < \frac{\delta}{2} \\ \frac{\delta}{2} + H - l \Leftrightarrow l > H - \frac{\delta}{2} \end{cases} \quad (10)$$

where *δ:* theoretical reinforcement influence thickness (15 cm);

*h':* effective reinforcement influence thickness (cm);

*H:* thickness of the reinforced layer (cm); and

*l:* distance between the geogrid layer and the bottom of the base course (cm).

The flowchart (Figure 2) summarizes the steps and the equations to evaluate the reinforced pavement performance.

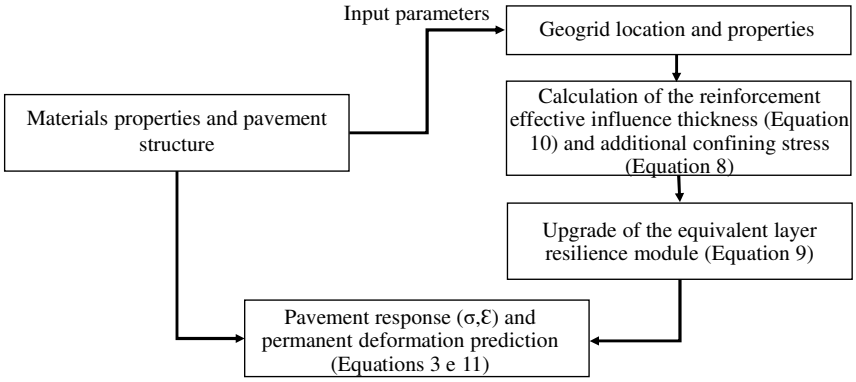


**Figure 2.** Flowchart to obtain the additional confining stress

## 3. MODEL VERIFICATION

According to Tang *et al*. (2013) and Kakuda *et al*. (2011), the greatest benefit of geogrid reinforcement is the permanent deformation reduction. Therefore, the proposed model was verified by comparing it with the experimental results of Kakuda (2010).

In a laboratory experiment conducted by Kakuda (2010) and, consequently, in the finite element model analysis in this paper, a traffic load of 550 kPa was applied to a plate with 15 cm radius. The pavement structure consists of a 20 cm granular base and a 50 cm clay subgrade. Three pavement conditions were analyzed: 1) without reinforcement; 2) with base/subgrade interface reinforced and 3) the middle of the base layer reinforced, as shown in Figure 3.

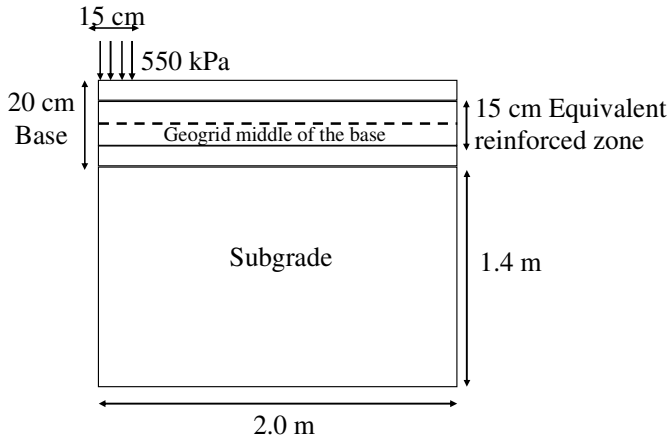


**Figure 3.** Structure analyzed in the model verification

Table 1 shows the materials properties from Kakuda (2010), which were utilized in this paper. To represent the nonlinear behavior of the base and subgrade material, the parameters in Equation 2 were used. Equation 3 represents the permanent deformation of both the base and subgrade. The geogrid was characterized by its stiffness (kN/m), Poisson's ratio and interface friction rate.

**Table 1** – Materials properties according to Kakuda (2010)

| **Material** | **Materials properties** | | | |
|---|---|---|---|---|
| Base | Resilient | | | |
| | **k1** | | **k2** | **k3** |
| | 508 | | 0,36 | -0.43 |
| | Permanent deformation | | | |
| | **ψ1** | **ψ2** | **ψ3** | **ψ4** |
| | 0.28 | -0.15 | 1.31 | 0.07 |
| Subgrade | Resilient | | | |
| | **k1** | | **k2** | **k3** |
| | 214 | | 0.41 | -0.05 |
| | Permanent deformation | | | |
| | **ψ1** | **ψ2** | **ψ3** | **ψ4** |
| | 0.21 | -0.24 | 1.35 | 0.04 |
| Geogrid | Poisson | 0.3 | Stiffness | 300 |
| | Friction coefficient | | | |
| | Base/Geogrid/Base | | Subgrade/Geogrid/Base | |
| | 0.50 | | 0.45 | |

*Calibrated values from Kakuda (2010).

Based on the flowchart in Figure 2, first the structure is analyzed without the reinforcement, then from its stress and strain response, the reinforcement influence thickness (h) and the new resilient modulus coefficients of the equivalent reinforced zone are obtained (k1, k2 and k3). Both parameters are illustrated in Figure 3 and quantified in Table 2.

**Table 2** – Reinforced zone resilient modulus coefficients

| | k1 | k2 | k3 | h (reinforcement influence thickness) |
|---|---|---|---|---|
| Without reinforcement | 508 | 0.36 | -0.43 | 0 |
| Interface | 910 | 0.34 | 0.44 | 7.5 |
| Middle of the base | 871 | 0.2 | -0.6 | 15 |

It is emphasized that to obtain the additional confining stress (Equation 8), a α = 1 (fully bonded geogrid) value was adopted. Moreover, in the reinforced structure simulations, the interface among layers assumed the following values: 1) μ is equal to 0 (not bonded), between the base and subgrade; 2) μ is equal to the values in Table 1, between the base/subgrade contact with geogrid and 3) μ is equal to 1 (bonded), between the base and equivalent reinforced zone.

From Equation 3, the stress state of a point provides its non-recoverable deformation as a function of the number of cycles. In this paper, the points adopted for the permanent deformation analysis are both on the loading line, located ¾ from the base thickness and 150 mm from the subgrade beginning. The total permanent deformation or rutting is the cumulative non-recoverable pavement deformation, considering all its layers, throughout its service life. This parameter is calculated by Equation 11, proposed by Barksdale (1972).

$$\delta_p = \sum_{i=1}^{n} (\varepsilon_{p(i)}.H) \tag{11}$$

where $\delta_p$: rutting (mm);

$\varepsilon_{p(i)}$: permanent deformation of the ith layer; and

$H$: thickness of the layer.

The comparison of experimental results with numerical results showed a significant reduction in permanent deformation. In the experimental results without reinforcement, the rutting for $4.10^5$ cycles was 2.0 mm, and in the reinforced cases, approximately 1.0 mm, providing a 50% reduction. For numerical results with the same number of cycles, the permanent deformation without reinforcement was 1.8 mm and 0.9 mm with reinforcement, also providing a 50% reduction. This comparison shows that the results from the proposed numerical model are compatible with the experimental results, as presented in Figure 4.

It can be seen in Figure 4, that the numerical model for all structures simulated showed a large increase in rutting at the beginning, and then gradually increasing rutting over the cycles. On the other hand, in the experimental analyses the same behavior is verified with the structure without reinforcement. However, with the geogrid reinforcement presence, this large increase in initial rutting was not observed. According to Chen *et al*. (2013), one of the reasons for this phenomenon is that the geogrid tends to delay the occurrence of constant plastic deformation.

The numerical modelling with the reinforcement positioned at the base/subgrade interface (Figure 4-b) showed lower values of rutting, when compared with other structures. This is because the base layer has low deformability and the subgrade is highly deformable. Therefore, for these simulated structures, the geogrid placed at the interface, with the function of protecting the subgrade, resulted in the best efficiency.

The pavement's response to permanent deformation is related to the layer's stress state, according to Equation 3. Figure 5 shows a graph with the stress reduction in the pavement layers, when comparing the conditions with and without reinforcement.

As shown in Figure 5, the numerical modelling results indicate a 43% vertical stress reduction in the base, when the geogrid is placed in the middle of the base, and a 27% reduction at the interface with the subgrade. Therefore, the efficiency of the reinforcement lies in the reduction of stresses in the base layer and, consequently, in permanent deformation.

Just as the reinforcement placed in the middle of the base is more efficient considering the reduction of vertical stress of this layer, the octahedral stress in the subgrade is lower when the geogrid is positioned at the interface.

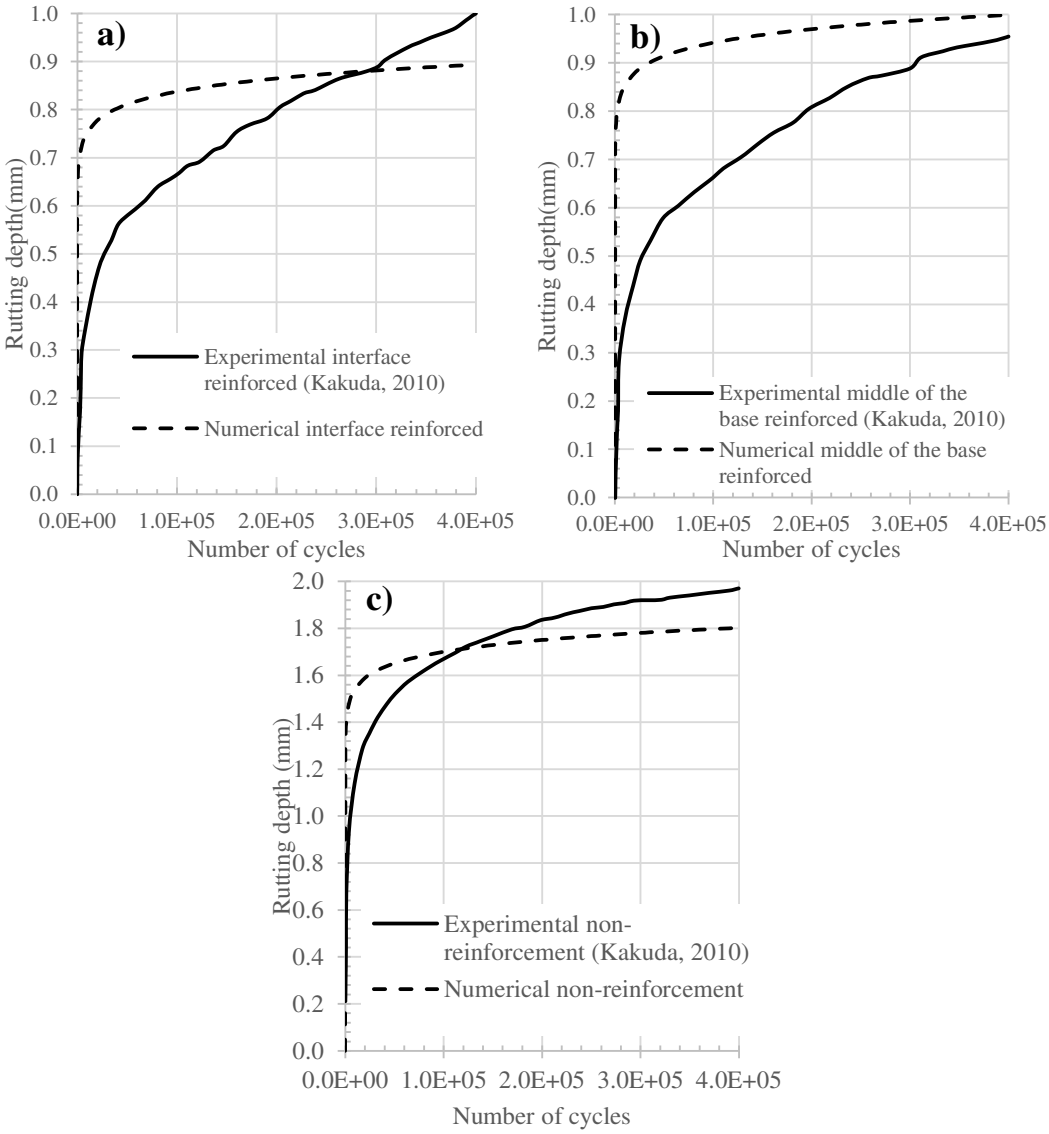


**Figure 4.** Comparison between numerical modeled and experimental analysis permanent deformation. a) Base/sub-grade interface reinforced; b) Reinforced at the middle of the base; c) Without reinforcement

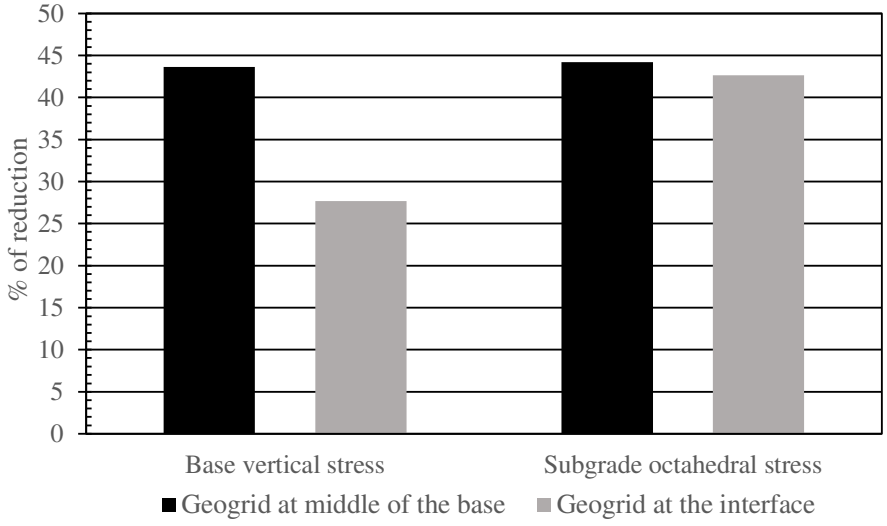


**Figure 5.** Reduction of vertical and octahedral stress with the presence of reinforcement

## 4. PARAMETRIC ANALYSIS OF PARAMETER SENSITIVITY

Two flexible pavement structures were simulated. The first consists of an asphaltic layer, a granular base, subbase, and soil subgrade. The second has an asphaltic layer, granular base, and soil subgrade. A reinforcement element (geogrid) was inserted in two conditions: in the middle of the base or at the interface with the subgrade.

### 4.1. Material properties and factorial design

The traffic load adopted in parametric analyses corresponds to a standard road axis with the following characteristics: axle load equal to 8.2 ton-force; tire pressure of 0.56 MPa; contact area radius of 10.79 cm; and wheel spacing of 32.4 cm. For the geometry of the load, the Huang (2004) principle was considered, which was idealized for finite elements, as shown in Figure 6.

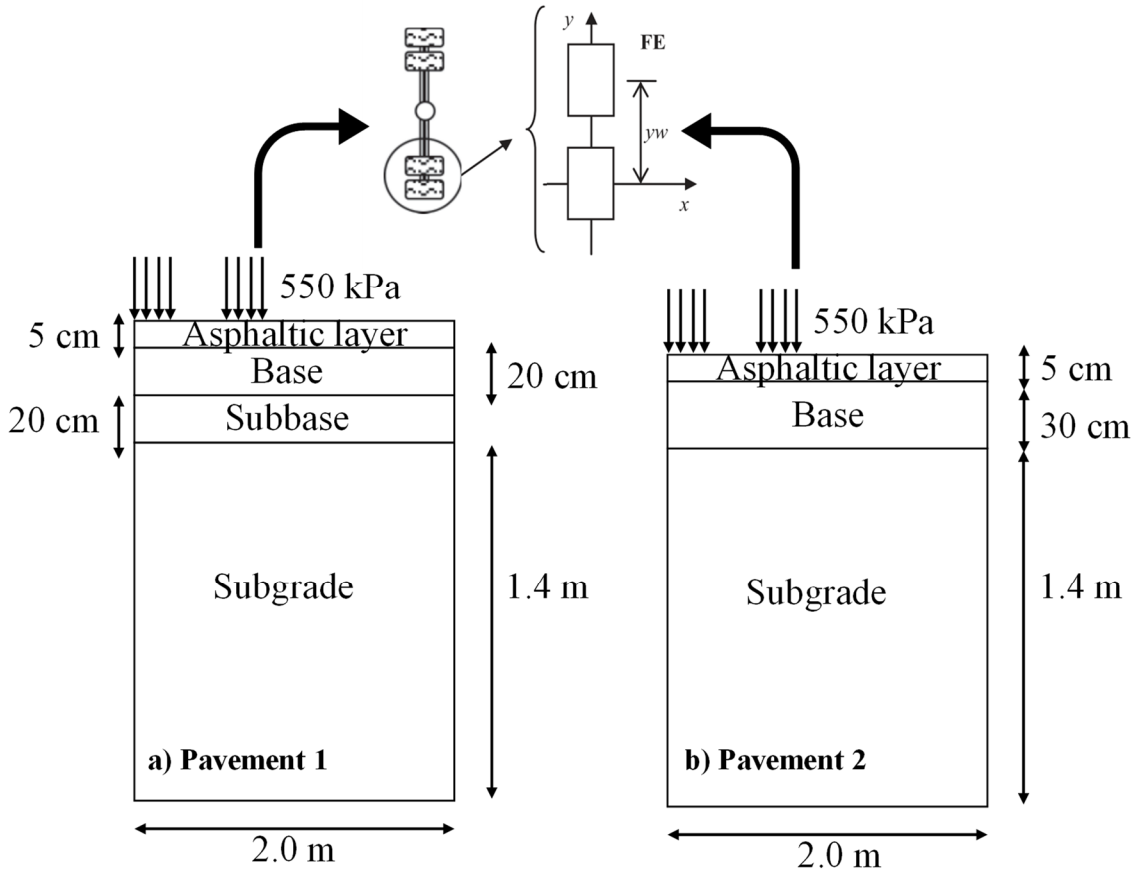


**Figure 6.** Analyzed pavement structures. a) Pavement 1 and b) Pavement 2

The materials properties adopted were according to MeDiNa program recommendations (Franco, 2019) and are presented in Table 3. As the aim of the paper is to evaluate geogrid reinforcement influence regarding the permanent deformation developed in layers below the asphaltic layer, a traffic load with an N value of $10^5$ was considered, making it possible to adopt a 5 cm asphaltic layer, which is the smallest thickness allowed by paving design instruction DER/SP (2006).

The choice of materials was influenced by the need to model a pavement structure that could have a high permanent deformation, with a rutting damage value close to the adopted limit of 10 mm. According to Al-Qadi *et al*. (2012), geogrid reinforcement is justified for pavements with

a subgrade CBR value below 7% and/or a thick granular base. Taking this indication into account, a granular base of simple graded gravel was adopted and, in the subgrade, a fine soil with high deformability. Therefore, the inclusion of geogrid and its influence in reducing strains/vertical stress of the layers is justified.

**Table 3** – Material properties of parametric analysis

| **Material** | **Materials properties** | | | |
|---|---|---|---|---|
| Asphaltic layer | Resilient modulus | | 5764 | |
| Granular base | Resilient | | | |
| | **k1** | | **k2** | **k3** |
| | 1149 | | 0.53 | -0.18 |
| | Permanent deformation | | | |
| | **ψ1** | **ψ2** | **ψ3** | **ψ4** |
| | 0.0868 | -0.2801 | 0.8929 | 0.0961 |
| Subbase | Resilient | | | |
| | **k1** | **k2** | **k3** | |
| | 446.5 | 0.262 | -0.086 | |
| | Permanent deformation | | | |
| | **ψ1** | **ψ2** | **ψ3** | **ψ4** |
| | 0.206 | -0.24 | 1.34 | 0.038 |
| Subgrade | Resilient | | | |
| | **k1** | **k2** | **k3** | |
| | 784.88 | 0.34 | - | |
| | Permanent deformation | | | |
| | **ψ1** | **ψ2** | **ψ3** | **ψ4** |
| | 0.097 | -1.6 | 1.9 | 0.063 |
| Geogrid | Poisson | 0.3 | Stiffness | 300/400 |
| | Interface α | | 0.8/1.0 | |
| | Friction coefficient | | | |
| | Base/Geogrid/Base | | Subgrade/Geogrid/Base | |
| | 0.50 | | 0.45 | |

The numerical simulations were planned considering a factorial design based on three factors and with two levels, with independent variables: x1 - geogrid stiffness; x2 - geogrid position; and x3 - α bonding coefficient of interface. A control simulation (0,0,0) was also considered without geogrid reinforcement. Figure 7 summarizes the numerical simulations performed.

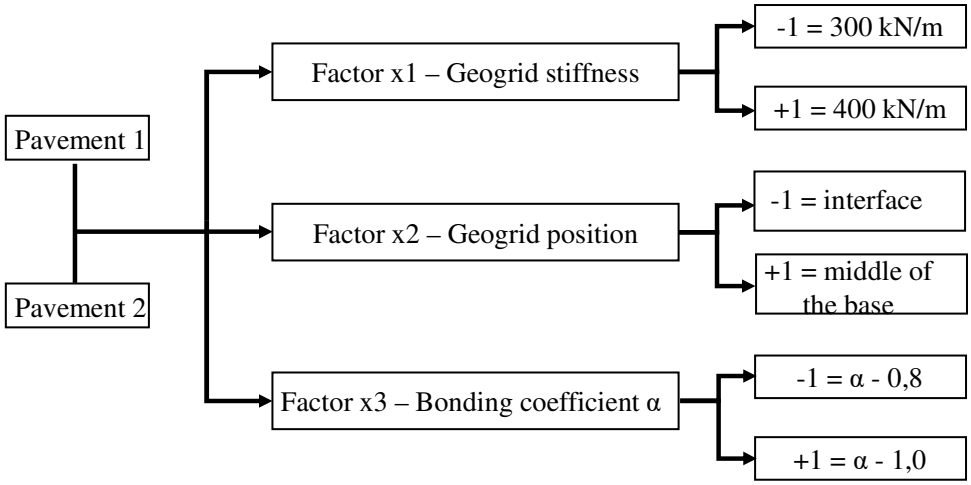


**Figure 7.** Simulated pavements

### 4.2. Effect of geogrid on permanent deformation

In the factorial experiment, the rutting damage pavement performance was adopted as a dependent variable, and it was analyzed separately regarding the subgrade, base, and total (subgrade+base). Therefore, the effect of the independent variables, previously described, on the structural response of the pavement was analyzed.

To obtain the rutting damage of each layer, the point within the layer under analysis was considered, in which the stress state is the most critical. The point referring to the second pair of wheels and between the wheels was assumed, positioned at ¾ of the base/subbase layer thickness and 500 mm below the subgrade.

Figure 8 shows the results of rutting in different simulated pavement structures, wherein: a) corresponds to pavement 1 and b) pavement 2. In both pavement structures, the geogrid reinforcement decreases the amount of rutting, when compared with the control condition (0; 0; 0).

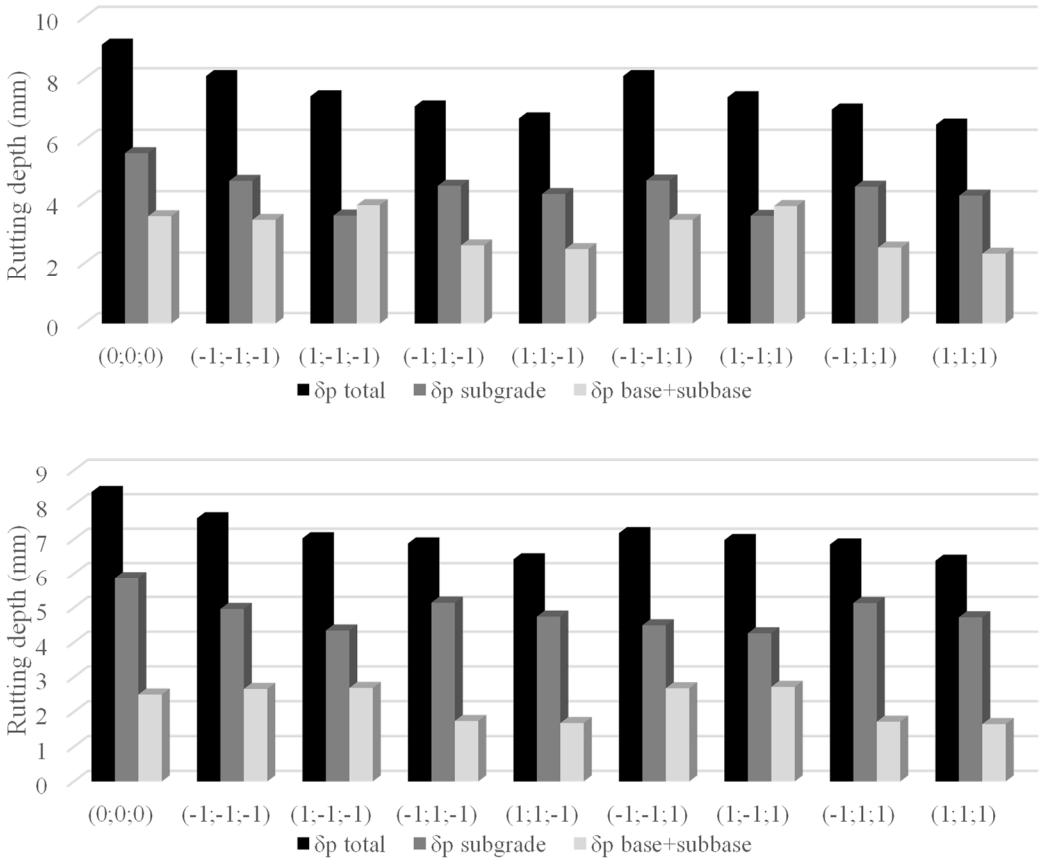


**Figure 8.** Permanent deformation. a) Pavement 1; b) Pavement 2

Regarding the total rutting, it can be seen from Figure 8 that the simulation with the factors (1; 1; 1) presented the best results for the two structures analyzed. The reduction in total rutting was 28.54% and 23.78% for structures 1 and 2, respectively.

The subgrade rutting had a value of 5.58 mm and 5.87 mm for structures 1 and 2 (Figure 8), respectively. Both values are greater than 5.0 mm, which is the recommended limiting from the MeDiNa program (Franco, 2019). For structure 1, all reinforced simulations showed subgrade rutting values lower than the limit, and the configuration (1; -1; 1) had better efficiency and

presented a subgrade rutting value of 3.54 mm, corresponding to a 36.56% reduction. In structure 2, only the configurations (-1; 1; -1) and (-1; 1; 1) did not present values lower than the recommended limit, and similar to structure 1, the configuration with the best efficiency was (1; -1 ; 1), presenting a reduction of 27.43% and a subgrade rutting value of 4.26 mm.

The regression equations obtained from the pavement response are shown in Table 4. Moreover, a 95% significance level was considered. It is emphasized that all values obtained for the p-value are lower than 5% and all equations resulted in a high $R^2$ (above 95%), indicating the strong correlation of factors associated with independent variables.

**Table 4** – Regression analysis of results

| **Pavement 1** | | | |
|---|---|---|---|
| **Parameter** | **R2** | **P-value** | **Equation** |
| $\delta_p$ total | 99.50% | 000088 | $\delta_{ptotal} = 7.29 - 0.28\ x1 - 0.46\ x2 - 0.04\ x3 + 0.06\ x1\ x2$ |
| $\delta_p$ base + subbase | 99.79% | 0.00024 | $\delta_{pbase+subbase} = 3.05 + 0.08\ x1 - 0.59\ x2 - 0.03\ x3 - 0.16\ x1\ x2$ |
| $\delta_p$ subgrade | 99.93% | 0.00004 | $\delta_{psubgrade} = 4.24 - 0.35\ x1 + 0.12\ x2 - 0.01\ x3 + 0.22\ x1\ x2$ |
| **Pavement 2** | | | |
| $\delta_p$ total | 98.03% | 0.04854 | $\delta_{ptotal} = 6.92 - 0.2\ x1 - 0.28\ x2 - 0.07\ x3 + 0.05\ x1\ x3 + 0.05\ x2\ x3$ |
| $\delta_p$ base + subbase | 99.93% | 0 | $\delta_{pbase+subbase} = 2.19 + 0.01\ x1 - 0.50\ x2 - 0.02\ x1\ x2$ |
| $\delta_p$ subgrade | 95.29% | 0.02486 | $\delta_{psubgrade} = 4.72 - 0.21\ x1 + 0.21\ x2 - 0.07\ x3 + 0.07\ x2\ x3$ |

Table 4 and Figure 8 show that the geogrid position (factor x2) is the factor with the greatest influence on rutting damage. Although both geogrid positions reduce the subgrade rutting, it can be observed that the geogrid position in the interface with the subgrade performs better. On the other hand, the geogrid positioned in the middle of the base/subbase has better efficiency reducing the base/subbase rutting.

Analyzing the reduction in base/subbase rutting with the presence of reinforcement in the middle of this layer, the sensitive analyses showed that the reinforcement in pavement 1 had a better efficiency than pavement 2 (Figure 8). Thus, the greater thickness of the base layer+ subbase present in structure 1 resulted in the best efficiency.

In general, the geogrid stiffness (factor x1) sensitivity analysis assumes values of 300 kN/m or 400 kN/m (Figure 7), which shows that the 400 kN/m stiffness value implies a higher addition confining stress (Equation 8) and resilient modulus from the reinforced equivalent layer (Equation 9), consequently, reducing the rutting damage. Considering the values in Table 4, it should be mentioned that in the pavement structures in which the reinforcement was placed in the middle of the base, factor x1 had less influence when placed in the interface with the subgrade.

Among the analyzed factors, the interface parameter (factor x3) had the least influence on rutting damage results (Table 4). However, this result is not negligible, because as factor x1 and factor x3, it changes the additional confining stress (Equation 8), the equivalent layer resilient modulus (Equation 9) and the rutting damage (Equation 11). Thus, according to Figure 8, a higher value of α results in a lower rutting value.

## 5. CONCLUSION

This paper presented a finite element model to simulate a geogrid reinforced flexible pavement. To do this, an analytical methodology was adapted to calculate the addition confining stress provided by the reinforcement, in which nonlinear behavior of the base and subgrade materials

was considered, throughout a UMAT introduction. The geotechnical materials properties (geogrid and soils) and interface were adopted from results available in the literature.

Initially, the rutting from experimental analysis results was used to calibrate the finite element numerical model proposed. A satisfactory fit between them were observed, therefore the numerical procedure developed in this paper has the potential to be used for geogrid reinforced flexible pavement design. However, other calibrations with experimental laboratory and field results must be performed to evaluate the numerical efficiency for other configurations.

It is noteworthy that the numerical curve modeled for rutting versus the number of cycles did not present the same shape as the experimental one, as the numerical curve is more accentuated in initial rutting values and reaches a constant N value smaller than the experimental curve.

In addition, a parametric study was carried out to verify the following parameter sensitivity: geogrid position, geogrid stiffness and geogrid/geotechnical material interface. From the results obtained, it can be concluded that the best position of the geogrid to reduce total rutting depends on which pavement layer has the greatest contribution to permanent deformation. Inserting the reinforcement into the middle of the base layer was efficient to reduce permanent deformation in this layer. Moreover, the geogrid positioned at base/subgrade or subbase/subgrade interface showed a better performance in reducing permanent deformations in the subgrade layer.

Among the factors evaluated in the regression analysis, it was observed that the increase in geogrid stiffness (parameter x1) had the greatest influence on additional confining stress and equivalent layer resilient modulus. Consequently, it resulted in less permanent deformation.

It is noteworthy that, in the regression analyses, the α bonding coefficient (parameter x3) between geogrid and geotechnical material had the least total rutting influence. However, it is a fundamental parameter which governs the interaction between materials, in other words, if it assumes a zero value there is no additional confining stress. Therefore, it is recommended to implement a correlation between the α bonding coefficient and granular material average diameter, geogrid installation conditions and geogrid properties.

Finally, it was concluded that the geogrid reinforcement element provides an improved pavement response, mainly by reducing the vertical stresses and, consequently, permanent deformation, which results in an increase in pavement service life.

**REFERENCES**

ABAQUS (2014) Getting Started with ABAQUS, Keywords Edition 14, 2014. Disponível em http://abaqus.software.polimi.it/v6.14/books/gsk/default.htm (acesso em 20/09/2019)

Abu-Farsakh, M. Y., Gu, J., Voyiadjis, G., Z., and Chen, Q. (2014). Mechanistic-empirical analysis of the results of finite element analysis on flexible pavement with geogrid base reinforcement. *International Journal of Pavement Engineering*, 15(9), 786-798. DOI: 10.1080/10298436.2014.893315.

Al-Qadi, I. L.; S. H. Dessouky; J. Kwon; e E. Tutumluer (2012) Geogrid-reinforced low-volume flexible pavements: pavement response and geogrid optimal location. *Journal of Transportation Engineering*, Nº138, p. 1083-1090. DOI: 10.1061/(ASCE)TE.1943-5436.0000409.

Barksdale, R. D (1972). Laboratory Evaluation of Rutting in Base Course Materials. In: *International Conference on Structural Design of Asphalt Pavements*, 3. Proceedings, London, pp. 161-174.

Bernucci, L. B.; L. M. G. Motta; J. A. P. Ceratti e J. B. Soares (2006) Pavimentação asfáltica: formação básica para engenheiros. Rio de Janeiro: PETROBRAS: ABEDA. p.504.

Chen, Q., Abu-Farsakh, M., Voyiadjis, G. Z., & Souci, G. (2013). Shakedown analysis of geogrid-reinforced granular base material. *Journal of Materials in Civil Engineering*, *25*(3), 337–346. DOI: 10.1061/(ASCE)MT.1943-5533.0000601

Costa, R.; R. Motta; J. Pires; P. Moraes; E. Moura; L. B. Bernucci e E. Mencher (2017) Avaliação estrutural *in situ* de uma via férrea reforçada com geogrelha. *Anais do XXXI Congresso Nacional de Pesquisa em Transportes*, ANPET, Recife, v. 1, p. 1098–1109.

DEPARTAMENTO DE ESTRADAS DE RODAGEM DO ESTADO DE SÃO PAULO. Instrução de projeto de pavimentação. IP-DE-P00/001. São Paulo, 2006. 53 p.

Franco, F. A. C. P. (2007). Método de dimensionamento mecanístico-empírico de pavimentos asfálticos – SisPav. Tese de Doutorado. COPPE/UFRJ, Rio de Janeiro, RJ, Brasil.

Franco, F. A. C. P. (2019). MeDiNa – Método de Dimensionamento Nacional. Manual de Utilização. Versão 1.1.3.0 Rio de Janeiro.

Gu, F.; X. Luo; R. Luo; R. L. Lytton; E. Y. Hajj; e R. V. Siddharthan (2016) Numerical modeling of geogrid-reinforced flexible pavement and corresponding validation using large-scale tank test. *Construction and Building Materials.* v. 122, p. 214-230. DOI: 10.1016/j.conbuildmat.2016.06.081

Guimarães, A. C. R. (2009). Um método mecanístico-empírico para a previsão da deformação permanente em solos tropicais constituintes de pavimentos*.* Tese de Doutorado. COPPE, Universidade Federal do Rio de Janeiro, Rio de Janeiro, RJ.

Guimarães, A.C.R., Motta, M.G. e Castro, C.D. (2018) Permanent deformation parameters of fine – grained tropical soils. *Road Materials and Pavement Design.* Vol. 20, No. 7. 1664-1681. DOI: 10.1080/14680629.2018.1473283

Hjelmstad, K. D. e E. Taciroglu (2000) Analysis and implementation of resilient modulus models for granular solids. *Journal of Engineering Mechanics,* v. 126, p. 821-830. DOI: 10.1016/(ASCE)0733-9399(2000)126:8(821)

Huang, Y. H. (2004). Pavement Analysis and Design. 2nd ed. Upper Saddle River, New Jersey, USA: Pearson Education Inc., Prentice Hall and Education Inc.

Kakuda, F. M. (2010). Desenvolvimento e a utilização de um equipamento de grandes dimensões na análise do comportamento mecânico de uma seção de pavimento sob carregamento cíclico. Tese de Doutorado. USP/EESC, São Carlos, Brasil.

Kakuda, F. M.; A. B. Parreira e G. T. P. Fabbri (2011) Análise de um pavimento reforçado com geossintético a partir de resultados de ensaio em equipamento de grandes dimensões. *Revista Transportes,* v. 19, p. 28-34. DOI: 10.14295/transportes.v19i2.532

Kwon, J.; E. Tutumluer; e M. Kim (2005) Development of a mechanistic model for geosynthetic-reinforced flexible pavements. *Geosynthetics International*, v. 12, p. 310-320. DOI: 10.1680/gein.2005.12.6.310

Marques, G. S. (2018) Avaliação da interação solo coesivo-geossintético por meio de ensaios de arrancamento monotônico e cíclico sob diferentes níveis de sucção e energia de compactação. Dissertação de Mestrado. Escola de Engenharia de São Carlos, Universidade de São Carlos, São Carlos, São Paulo, Brasil.

Nazzal, M. D., Abu-Farsakh, M. Y., and Mohammad, L. N. (2010). Implementation of a critical state two-surface model to evaluate the response of geosynthetics reinforced pavements. *International Journal of Geomechanics,* 10(5), 202-212. DOI: 10.1061/(ASCE)GM.1943-5622.0000058

Perkins, S. W. e Ismeik, M. (1997) A synthesis and evaluation of geosynthetic-reinforced base course layers in flexible pavements. *Geosynthetic International*, v. 4, No. 6, pp. 549-621. DOI: 10.1680/gein.4.0106

Perkins, S. W. (2004). Development of design methods for geosynthetic- reinforced flexible pavements. DTFH61-01-X-00068, U.S. Department of Transportation, Federal Highway Administration, Wash- ington, DC.

Perkins, S. W.; B. R. Christopher; E. L. Cuelho; G.R. Eiksund; C. S. Schwartz e G. Svano (2009) A mechanistic-empirical model for base-reinforced flexible pavements. *International Journal of Pavement Engineering*, v. 10:2, p. 101-114. DOI: 10.1080/10298430802009646

Santos, A. G.; R. K. M. Assis e L. J. Fernandes Jr (2019) Efeito da aderência entre camadas na previsão de desempenho de pavimentos asfálticos. *Revista Transportes,* v. 27, p. 89-101. DOI: 10.14295/transportes.v27i2.1597

Schuettpelz, C., Fratta, D., & Edil, T. B. (2009). Evaluation of the Zone of Influence and Stiffness Improvement from Geogrid Reinforcement in Granular Materials. *Transportation Research Record*, 2116(1), 76–84. DOI: 10.3141/2116-11

Tang, X., Stoffels, S. M., & Palomino, A. M. (2013). Resilient and permanent deformation characteristics of unbound pavement layers modified by geogrids. *Transportation Research Record*, *2369*, 3–10. DOI: 10.3141/2369-01

Tang, X., Stoffels, S. M., & Palomino, A. M. (2016). Mechanistic-empirical approach to characterizing permanent deformation of reinforced soft soil subgrade. *Geotextiles and Geomembranes*, *44*(3), 429–441. DOI: 10.1016/j.geotexmem.2015.06.004

Uzan, J. (1988) Characterization of granular materials. *Transportation Research Record.* Transportation Research Boards, Washington, D.C., p. 52-59.

Vertematti, J. C. (2015) Manual brasileiro de geossintéticos. *Editora – São Paulo: Bluncher*. 2ª Edição, pp. 570.

Yang, X., & Han, J. (2013). Analytical model for resilient modulus and permanent deformation of geosynthetic-reinforced unbound granular material. *Journal of Geotechnical and Geoenvironmental Engineering*, 139(9), 1443–1453. DOI: 10.1061/(ASCE)GT.1943-5606.0000879

Yoder, E. J., e Witczak, M. W. (1975). Principles of pavement design. 2nd edition, John Wiley, and Sons, 711p.